

# Toward Unveiling Putative Binding Sites of Interleukin-33: Insights from Mixed-Solvent Molecular Dynamics Simulations of the Interleukin-1 Family

Tan Thanh Mai, Thua-Phong Lam, Long-Hung Dinh Pham, Kim-Hung Nguyen, Quoc-Thai Nguyen, Minh-Tri Le, and Khac-Minh Thai\*



Cite This: <https://doi.org/10.1021/acs.jpcb.4c03057>



Read Online

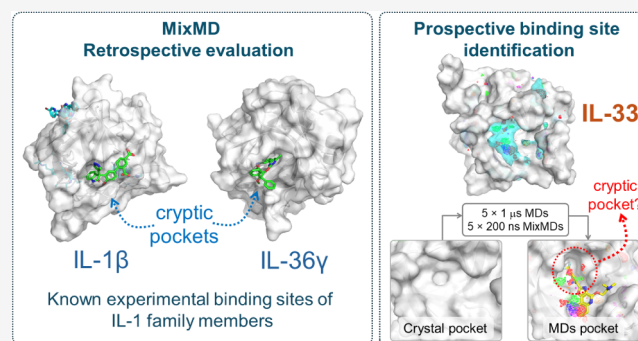
ACCESS |

Metrics & More

Article Recommendations

Supporting Information

**ABSTRACT:** The interleukin (IL)-1 family is a major proinflammatory cytokine family, ranging from the well-studied IL-1s to the most recently discovered IL-33. As a new focus, IL-33 has attracted extensive research for its crucial immunoregulatory roles, leading to the development of notable monoclonal antibodies as clinical candidates. Efforts to develop small molecules disrupting IL-33/ST2 interaction remain highly desired but encounter challenges due to the shallow and featureless interfaces. The information from relative cytokines has shown that traditional binding site identification methods still struggle in mapping cryptic sites, necessitating dynamic approaches to uncover druggable pockets on IL-33. Here, we employed mixed-solvent molecular dynamics (MixMD) simulations with diverse-property probes to map the hotspots of IL-33 and identify potential binding sites. The protocol was first validated using the known binding sites of two IL-1 family members and then applied to the structure of IL-33. Our simulations revealed several binding sites and proposed side-chain rearrangements essential for the binding of a known inhibitor, aligning well with experimental NMR findings. Further microsecond-time scale simulations of this IL-33-protein complex unveiled distinct binding modes with varying occurrences. These results could facilitate future efforts in developing ligands to target challenging flexible pockets of IL-33 and IL-1 family cytokines in general.



## INTRODUCTION

Following two decades of research into its origin, structure, biological functions, and roles in various pathological conditions, interleukin (IL)-33 has emerged as a highly promising target for therapeutic interventions in inflammatory and autoimmune conditions. IL-33 is the most recently discovered member of the IL-1 family, distributed in tissues of the respiratory tract, gastrointestinal tract, skin, and central nervous system.<sup>1,2</sup> It is synthesized intracellularly in a full-length form consisting of 270 residues (IL-33<sub>1–270</sub>), functioning as a nuclear factor through its N-terminal domain (Met1–Thr65) with the capability to bind to chromatin.<sup>2</sup> Cleaved by immune cell-derived proteases and released extracellularly, the mature form of IL-33 (IL-33<sub>112–270</sub>) is mostly studied for its activity as a proinflammatory cytokine. In a steady state, IL-33 acts as an “alarmin”, facilitating homeostasis and tissue repair, as well as modulating immune type 2 responses. Nonetheless, its overexpression can promote inflammation, allergy, and cancer metastasis. IL-33<sub>112–270</sub> only exhibits activity through its protein–protein interaction (PPI) with the membrane-bound ST2 receptor of target cells, particularly immune cells.<sup>3</sup> Similar to other IL-1 family members, the IL-33/ST2 complex needs

to additionally bind with the IL-1RαCp coreceptor to form a heterotrimer to activate the MyD88-dependent signaling pathway inside the target cell and induce biological responses.<sup>4</sup> IL-33 affects a diverse array of cell types, encompassing mast cells, eosinophils, basophils, type 2 helper T cells (T<sub>H</sub>2), regulatory T cells (Treg), and type 2 innate lymphoid cells (ILC2).<sup>5</sup>

The cytokine form of IL-33 interacts with the extracellular domain of ST2 on two separate interface surfaces, as described by Liu et al. (Figure 1A).<sup>6</sup> Site 1 of IL-33 contains polar and negatively charged residues (notably Glu144, Glu148, Asp149, and Asp244). These residues form salt bridges with positively charged residues on the surface of ST2 and are crucial for the binding of IL-33 to ST2. On the other hand, Site 2 contains a

Received: May 9, 2024

Revised: July 27, 2024

Accepted: August 13, 2024

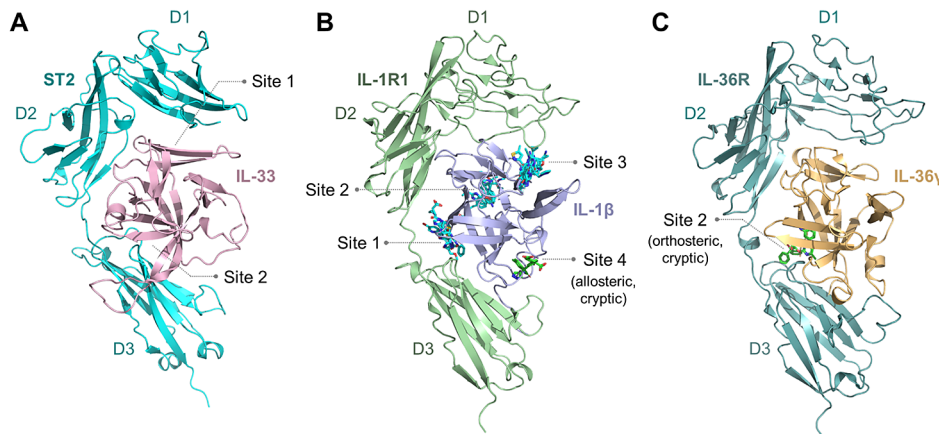


**Figure 1.** Crystal structures of IL-33, IL-1 $\beta$ , and IL-36 $\gamma$  in complex with their specific receptors. (A) IL-33 (light pink) interacts with the ST2 receptor (cyan) at two distinct interfaces (PDB 4KC3) described by Liu et al.<sup>6</sup> (Site 1 and Site 2). (B) IL-1 $\beta$  (light blue) also interacts with IL-1R1 (pale green) in a similar manner (PDB 4DEP). Here, we illustrate the four binding sites on IL-1 $\beta$  as described by Nichols et al.<sup>18</sup> Fragment binders, depicted as cyan sticks, are located at Sites 1 and 3 (correspond to Sites 1 and 2 of the IL-33/ST2 PPI), and at Site 2 (where monoclonal antibody canakinumab binds and neutralizes IL-1 $\beta$ ). Inhibitor 2 binds to IL-1 $\beta$  at allosteric Site 4, which is also a cryptic site. (C) The apo structure of IL-36 $\gamma$  (PDB 4IZE) is displayed alongside a putative structure of IL-36R, a homology model for this receptor was built using SwissModel for illustrative purposes, with IL-1R1 (PDB 4DEP) serving as the template. Ligand A-552, shown as a green stick, binds to IL-36 $\gamma$  within a cryptic pocket at a position corresponding to Site 2 of the IL-33/ST2 PPI.

mixture of hydrophilic and hydrophobic interactions contributed by Glu165, Tyr163, and Leu182. The total surface area of protein–protein interaction (PPI) at the two sites on IL-33 is nearly 1800 Å<sup>2</sup>, posing an inherent challenge for the discovery of small-molecule inhibitors of PPI.<sup>6</sup>

There is still a debate about whether IL-33 is helpful or harmful, for example, in the context of infections or cancer.<sup>7,8</sup> In certain conditions, such as active inflammatory bowel disease and graft-versus-host disease, the soluble ST2 receptor (sST2) is the main contributor to the pathology, as it blocks the interaction between IL-33 and the transmembrane ST2 receptor.<sup>5,9–11</sup> However, blocking the IL-33/ST2 signaling has been shown to have a clear positive impact on inflammatory, allergic, and autoimmune diseases. In efforts to discover new drugs targeting this cytokine, several monoclonal antibodies neutralizing IL-33 have been developed, such as torudokimab and etokimab for the treatment of atopic dermatitis, and itepikimab and tozorakimab for COPD.<sup>12–15</sup> Additionally, several types of IL-33 traps have also been reported, such as the agents described in the patent WO2014/152195A1, in the study by Nguyen et al., and by Murphy et al.<sup>16,17</sup>

Despite the challenges, the appeal of small-molecule inhibitors to medicinal chemists remains undiminished, largely due to their oral bioavailability, cost-effectiveness, and predictable pharmacokinetic and pharmacodynamic profiles. This interest has extended to the realm of IL-33 inhibition. BTB11086 has been introduced as the first small-molecule binder on IL-33, leading to the development of its derivative 7c (*N,N*-dimethyl-2-((2-(4-(trifluoromethyl)phenyl)oxazolo[4,5-*c*]quinolin-4-yl)oxy)ethan-1-amine) with stronger binding affinity and demonstrating inhibitory efficacy on IL-33 activity in the human mast cell line. Chemical shift perturbation (CSP) observed in the NMR spectrum reveals that these low molecular weight molecules bind to IL-33 at Site 2 of the PPI interface with ST2.<sup>19,20</sup> Additionally, at this very site, several potential natural-origin hit compounds, including heterocyclic and triterpenoid saponin compounds, have been reported.<sup>21,22</sup> Conversely, at Site 1, we reported several hit

compounds with folate structures identified through a virtual screening using the PPI mimicry pharmacophore approach.<sup>23</sup>

In summary, previous studies using structure-based virtual screening were conducted based on the assumption that the PPI interface (Site 1 or Site 2) is an appropriate starting point without proper systematic assessment of their druggability. By conducting a thorough survey of the complexes formed by other IL-1 family members with small-molecule ligands on the Protein Data Bank (PDB), especially IL-1 $\beta$  and IL-36 $\gamma$ , we observed that several pockets outside the PPI interface could also serve as druggable binding sites.<sup>18,24–26</sup> These pockets can be referred to as allosteric sites. More interestingly, in certain cases, the binding pocket is not present in the unbound (apo) form of the protein and only becomes accessible upon ligand binding, leading to the identification of what are known as cryptic pockets in IL-1 family cytokines. This insight establishes a foundational framework for exploring potential binding sites on IL-33. Considering the structural similarities within the IL-1 family, it is hypothesized that IL-33 could similarly accommodate small-molecule ligand binding sites, expanding the scope for targeting this cytokine.

Indeed, binding site identification is a critical step in target validation in the new drug discovery pipeline. However, exploring druggable cavities on protein surfaces is not straightforward, especially in the case of proteins involved in PPIs like IL-33. Currently, binding site identification for proteins without a known cocrystallized ligand relies on three primary methodologies: sequence-based, structure-based, and knowledge-based.<sup>27</sup> Structure-based techniques are most commonly employed and encompass both geometry-based tools (e.g., SiteMap, MOE Site Finder, Fpocket, DoGSiteScorer, CASTp) and energy-based tools (e.g., AutoSite, FTMap).<sup>28–34</sup> Additionally, machine and deep learning tools, such as P2Rank, DeepSite, DeepPocket, and PocketMiner, are increasingly being utilized.<sup>35–38</sup> However, none of these techniques can address the flexibility of proteins, especially in the case of proteins involved in PPIs. The broad and shallow nature of PPI interfaces further complicates detection by traditional binding site identification tools, which may not

adequately identify orthosteric, allosteric, or cryptic pockets. As a solution, cosolvent molecular dynamics (MD) simulations are suggested to address these limitations, offering a more dynamic approach to understanding protein flexibility and revealing potential binding sites.<sup>27</sup>

Among the reported cosolvent MD approaches, MixMD stands out as an effective method for mapping binding hot spots that can replicate experimental results from the multiple-solvent crystal structure (MSCS) technique.<sup>39</sup> MixMD is characterized by the use of organic water-dispersible probes, thus eliminating the need for artificial repulsive terms to prevent probe aggregation.<sup>40</sup> The MixMD protocol has been continuously improved, from using binary solvent mixtures at lower concentrations but with more effective hot-spot mapping, to developing a ranking function for binding sites.<sup>41,42</sup> Additionally, this technique is particularly notable for allowing organic molecules to directly compete with water molecules while accommodating the full range of protein flexibility, presenting a unique advantage.<sup>43</sup> It has proven effective in studies involving viral proteases and enzymes from the kinase family.<sup>41,44,45</sup> Ghanakota et al. expanded on the MixMD procedure to evolve it into MSMD, subsequently applying this method to PPI targets.<sup>46</sup> Noticeably, Yuan et al. also employed cosolvent MD in their mapping analysis to successfully identify ST2 receptor inhibitors.<sup>47</sup> Inspired by these advancements, we embarked on our application of MixMD to investigate binding sites on members of the IL-1 family. To underscore the applicability of MixMD in studying cytokines, the method was employed on the apo structures of IL-1 $\beta$  and IL-36 $\gamma$  using a set of five probes (isopropanol, acetonitrile, pyrimidine, benzene, and N-methylacetamide), and binding hot-spot maps were compared with cocrystallized ligand positions in experimental holo-structures. A similar protocol was then applied to the crystal structure IL-33 to comprehensively explore potential ligand binding sites. The results of MixMD were also compared with those of other binding site detection methods that use the protein's static structure. A binding pocket identified as the top-ranked by our postcosolvent MD analysis aligns with the binding site of compound 7c proposed by Kim et al.<sup>19</sup> We performed extensive MD simulations on IL-33 in the presence of 7c in this pocket, achieving a total trajectory length of 5  $\mu$ s. Subsequently, the combination of MM-GBSA binding free energy calculations and conformational clustering from MD data revealed a high druggability binding site model for IL-33. The consensus-binding sites we propose here could serve as a potential basis for further structure-based drug design efforts against IL-33.

## METHODS

### Retrieval of IL-1 Cytokines with Known Bound Small Molecules.

To assess the effectiveness of MixMD in the context of the IL-1 family, we first queried the RCSB Protein Data Bank for crystal structures of human IL-1 family cytokines that have been cocrystallized with small molecules utilizing their respective Uniprot IDs. The search results are detailed in the Table S1. In this study, we opted for the apo form (or the receptor-bound form) of these cytokines, aiming to possibly harness MixMD's capability in capturing real-life binding events and predicting potential binding sites where prior knowledge is limited. In the case where both the crystal structures of the apo-form and receptor-bound form of a cytokine exist, we chose the receptor-bound form to better

resemble the scenario of IL-33, for which only the receptor-bound form is available. This resulted in two cytokine complexes being chosen as initial test cases, as depicted in Figure 1B,C, including IL-1 $\beta$  (PDB 4DEP, resolution 3.10 Å)<sup>48</sup> and IL-36 $\gamma$  (PDB 4IZE, resolution 2.00 Å).<sup>49</sup> Subsequently, we applied MixMD to explore the binding sites on the IL-33 crystal structure (PDB 4KC3, resolution 3.27 Å).<sup>6</sup>

### Preparation of IL-1 $\beta$ , IL-36 $\gamma$ , and IL-33 Structures.

Prior to all-atom MD simulations, the protein structures of the cytokines were isolated and prepared using the QuickPrep function integrated into the MOE 2022.02 program.<sup>50</sup> In particular, the protonation state of the side chains was assigned, the nonstandard residues were transformed back to their natural form, and the missing loops of the cytokines were remodeled automatically. As we assume these loops might fully fluctuate in the simulation environment, no postmodeling analysis of this initial protein conformation was conducted. The prepared protein structures are provided as Supporting Materials.

**Mixed-Solvent Molecular Dynamics (MixMD) Simulations.** MixMD simulations were conducted using the Amber22<sup>51</sup> program, following the protocol developed by Carlson et al.<sup>39,52</sup> Specifically, the protein backbone was parametrized using the Amber ff14SB<sup>53</sup> force field using the tLEAP program, while the force field parameters of the probes (isopropanol – IPA; acetonitrile – ACN; pyrimidine – 1P3; N-methylacetamide – NMA) were retrieved from previous studies of Lexa et al.<sup>52</sup> These probes were employed to identify key aromatic, hydrophobic, and hydrogen bond interactions on binding sites of protein surfaces, as demonstrated in previous studies.<sup>27,44,54</sup> Additionally, we also included benzene (BNZ) as an aromatic and hydrophobic probe in our simulations. Although the authors of MixMD previously disregarded BNZ as a good cosolvent without the use of repulsive force due to aggregation occurring during the MD simulation,<sup>52</sup> we argue that the OPLS parameters used were not well optimized. In this study, we employed the parameters of BNZ developed by Accelera Lab (Table S2),<sup>55</sup> which was afterward proved to be water-miscible in the condition used (Figure S1). After parametrization, a 7-Ångstrom shell of chemical probes was placed surrounding the protein surface, before the whole system was placed in a cubic water box containing adequate TIP3P water molecules to achieve a probe concentration of approximately 5% (v/v). To attain a neutral charge, sodium or chloride ions were introduced. The Supporting Information includes details on each system's probe and water molecule quantities (Table S3).

Prior to MD production, each system underwent a series of seven equilibrium stages. The initial stage involved a first round of minimization with a harmonic restraint force of 500 kcal/mol·Å<sup>2</sup>, comprising 250 cycles of the steepest descent algorithm followed by 4750 cycles of the conjugate gradient algorithm. Afterward, a second round of 2500-step unrestrained minimization was conducted. Following minimizations, the system underwent gradual heating from 10 to 300 K over 100 ps with a 10-kcal/mol·Å<sup>2</sup> restraint force on protein atoms. Once the target temperature was reached, three consecutive NPT equilibria were performed, each lasting 20 ps, to progressively reduce the restraining force on the protein backbone under constant pressure. Subsequently, the system underwent another NPT equilibration for 2 ns with the protein structure being fully flexible. These equilibria were crucial as

full protein flexibility is essential for proper hotspot mapping and site detection.<sup>39</sup>

Ten independent 20 ns simulations in the NPT ensemble were carried out using the pmemd.cuda module<sup>56</sup> of Amber22, summing up a cumulative simulation time of 200 ns for each probe. Throughout the simulations, the SHAKE<sup>57</sup> algorithm was applied to restrain all hydrogen-containing bonds, allowing a time step of 2 fs to be used. Meanwhile, the temperature of 300 K was maintained through the Andersen thermostat, and a pressure of 1 bar was controlled using the Berendsen barostat. Nonbonded interactions cutoff was set at 10.0 Å and long-range electrostatics were managed through Particle Mesh Ewald summation.

**Processing and Analysis of MixMD Results.** The molecular system requires an equilibration period in MD simulation. In this study, the last 5 ns from each of the ten simulation runs for every organic probe were combined into a unified trajectory. Subsequently, this trajectory was binned onto a 0.5 × 0.5 × 0.5 Å grid using the cpptraj module<sup>58</sup> of AmberTools23. The duration of the analysis window was chosen based on a comparative study by Lexa and Carlson.<sup>59</sup> Only the center-of-mass atom of the probes is considered in this calculation. Following this, an in-house Python script was employed to transform raw bin counts ( $x$ ) at each grid point into normalized  $z$ -values. These  $z$ -values denote the number of standard deviations ( $\sigma$ ) away from the mean background noise level ( $\mu$ ). Thus, a higher  $z$ -value indicates a longer residency time of the chemical probe at a specific grid point. This normalization step also allows us to compare the results across different simulation runs and chemical probes. The normalized occupancy map could then be examined and visualized on PyMOL<sup>60</sup> in the same manner as electron density maps. These maps are color-coded as BNZ—red, 1P3—magenta, IPA—blue, ACN—orange, and NMA—green. The normalization equation is given by formula 11:

$$z = \frac{x - \mu}{\sigma} \quad (1)$$

Hotspot ranking and automated site prediction were conducted using a modified version of MixMD ProbeView from Carlson's group.<sup>42</sup> Adaptations were made to implement the MixMD ProbeView program which was originally written in Python 2, for the Python 3 environment of PyMOL. In brief, MixMD ProbeView takes pseudo-PDB files generated from the grid command of cpptraj as input and employs the DBSCAN clustering algorithm<sup>61</sup> on the density of occupancy. The default parameters (occupancy cutoff = 0.1;  $\epsilon = 3$  Å; minimum number of points = 10) were used in the cases of IL-1 $\beta$  and IL-36 $\gamma$ . As for the case of IL-33, due to the higher signal observed, a higher occupancy cutoff of 0.2 was used. Site ranking was based on either the maximum occupancy within each cluster or the sum of occupancy within the same cluster.

**Molecular Docking and Large Time Scale MD Simulation of a Known IL-33 Inhibitor.** In addition to MixMD simulations, an alternative strategy was employed to gain deeper insights into the mechanism of action of a known IL-33 orthosteric inhibitor (compound 7c).<sup>19</sup> Briefly, compound 7c was docked into the orthosteric binding site of IL-33, denoted as Site 2 by Liu et al.,<sup>6</sup> utilizing AutoDock Vina 1.1.2.<sup>62</sup> The preparation of the protein and ligand was conducted as previously reported studies by our group,<sup>63,64</sup> with the docking grid box being detailed in Figure S2. To comprehensively explore potential initial binding poses within

the binding site, a high exhaustiveness of 1024 was used. Following molecular docking, the first docking pose was subjected to five independent long-time scale MD simulations, each spanning 1 μs and totaling 5 μs of simulation time. Before MD production, the ligand was parametrized with the GAFF2<sup>65</sup> force field using the antechamber module,<sup>66</sup> which was then combined with the protein topology using tLEAP. The solvation and neutralization stages and the equilibrium process were implemented following the above-described procedures.

After MD production, ProLIF<sup>67</sup> was used to encode the protein–ligand interactions as fingerprints along the trajectories. The MMPBSA.py program<sup>68</sup> was utilized to estimate the end-state binding free energy of compound 7c within the IL-33 complex, employing the MM-GBSA method. A modified script implementing Quality Threshold Clustering with a cutoff of 3.0 Å based on González-Alemán et al.<sup>69</sup> has been used to cluster the heavy atoms of the ligand during the simulations. PoseEdit<sup>70</sup> was used for 2D protein–ligand interaction analysis and PyMOL<sup>60</sup> was used for visualization in 3-dimension.

## RESULTS

**MixMD Effectively Detects Experimental Binding Sites of IL-1 Family Cytokines.** Search strategies on the Protein Data Bank resulted in two interleukin systems selected as retrospective case studies to examine the capabilities of MixMD in mapping binding sites on IL-1 cytokines. These test cases present significant challenges due to the experimental ligands binding at allosteric sites or even cryptic pockets. The efficacy of MixMD in identifying the binding sites on IL-1 $\beta$  and IL-36 $\gamma$  is described in the subsequent subsections.

**Interleukin-1 $\beta$ .** IL-1 $\beta$ , along with IL-1 $\alpha$ , are the original members of the IL-1 family. IL-1 $\beta$  interacts with its receptor IL-1R1 through two distinct binding sites, similarly to IL-33.<sup>71</sup> The inhibition of the IL-1 cascade by biologic agents has demonstrated significant benefits in treating various inflammatory diseases, including rheumatoid arthritis, gout, and diabetes.<sup>72</sup> Recently, Nichols et al. conducted a fragment-based X-ray crystallography screening, which has revealed several scaffolds of weak binders of IL-1 $\beta$ .<sup>18</sup> Three binding sites were detected on the surfaces of IL-1 $\beta$  (Figure 1B), which were also mapped by MixMD in our study. For ease of comparison, we will use the same site numbering as that of Nichols's original paper.<sup>18</sup>

In particular, Site 1, the orthosteric site that interacts with the domain D3 of IL1-R1,<sup>71</sup> was reported to interact with fragments by the amino and carboxyl groups of Met148 and be capable of accommodating a wide range of aromatic rings in the central hydrophobic groove.<sup>18</sup> In our analysis, MixMD was able to map all of these features (Figure 2A), with BNZ (red) mapping the hydrophobic center and NMA (green) identifying hydrogen-bond donor and acceptor features. Additionally, simulations also revealed a novel hotspot near the reported site, formed by the side chains of Thr147, Glu149, and Arg11, suggesting its potential use in guiding the growing direction of reported binders for enhanced affinity (Figure 2A). Site 2 is a small cavity that coincides with the binding site of canakinumab, an anti-IL-1 $\beta$  antibody,<sup>18</sup> and was mapped by three out of five probes (BNZ, NMA 1P3, see Figure 2B). Likewise, the close hotspots surrounding Gln39 can also be used to guide the optimization of the fragments to enhance binding affinity. The last site (Site 3), located near the PPI interface of IL-1 $\beta$  and domain D1-D2 of IL-1R1, was

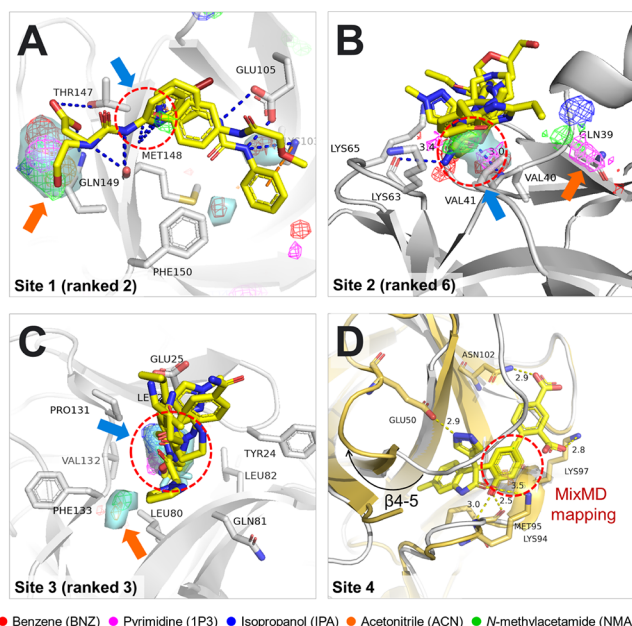


**Figure 2.** Mapping of binding hotspots as identified by MixMD (at  $z = 20\sigma$ ), on the four ligand binding sites of IL-1 $\beta$ . Mesh representations in different colors indicate mappings of the five probe types while the cyan surface represents clustering results from MixMD ProbeView. Panels A, B, and C show bound ligands reported by Nichols et al.<sup>18</sup> at each site. Blue arrows highlight the mapping of hotspots using MixMD, indicating hydrogen bonds with Met148 (A), the small cavity involved in canakinumab binding (B), and the hydrophobic groove accommodating the largest number of binders as per Nichols et al. (C). The orange arrows suggest growing directions for fragments for improved potency. Panel D shows a superimposition of IL-1 $\beta$  in its apo form (white – PDB: 4DEP) and holo form with compound 2 (yellow – PDB: 8C3U).<sup>25</sup>

previously reported with the highest number of fragments bound.<sup>18</sup> During MixMD simulations, this site was also successfully mapped by all of the probes, except for BNZ (Figure 2C). Collectively, MixMD was able to map all the experimentally reported binding sites reported by Nichols et al.<sup>18</sup> as well as suggesting growing directions for fragment-based drug development. Nevertheless, it should be kept in mind that all the reported binders only bind to IL-1 $\beta$  in crystal-soaking experiments without being reported for their inhibitory activity against the IL-1 pathway. In theory, Site 1 remains a promising binding site for inhibiting IL-1 $\beta$ /IL-1R PPI and, consequently, inhibiting this pathway, and therefore our MixMD results could be used to guide the growing direction of these fragments. Our MixMD results offer insights for enhancing fragment affinity, as demonstrated by Gupta and Carlson.<sup>73</sup>

More recently, a novel allosteric inhibitor of IL-1 $\beta$  has been reported, unveiling a cryptic binding site (Site 4) distinct from the previously described sites.<sup>25</sup> Subsequent X-ray crystallography investigations have identified several structural requirements for IL-1 $\beta$  inhibition, elucidating the compound's mechanism of action through allosteric modulation. Notably, the binding of this molecule necessitates the rearrangement of IL-1 $\beta$ , with the most significant change being the displacement of loop  $\beta$ 4– $\beta$ 5 (residues 45–55) by up to 11 Å from its receptor-bound conformation. This ligand-bound state is incompatible with binding to its IL-1R1 receptor, providing insight into the antagonistic activity of the compound. Ideally,

MD simulations would sample the open conformation allowing chemical probes to engage with core hydrophobic residues (Val3, Val47, Pro57, Met95, and Val100). Unfortunately, conventional MixMD failed to map the binding site proposed by Hommel et al., with only ACN (orange) and NMA (green meshes – Figure 2D) partially occupying the desired site. Mapping at a lower signal-to-noise ratio (Figure S3) revealed that probe capture was limited to the outer part of the ligand (biphenyl scaffold), without deep penetration to the core hydrophobic region. The clustering of MD trajectories based on binding pocket residues also suggested that conventional MD simulations may insufficiently sample the required conformation. In contrast to the case of IL-36 $\gamma$ , where only side chain reorganization is necessary, the cryptic site of IL-1 $\beta$  demands the movement of a larger loop and backbone rearrangement, potentially requiring a longer simulation time scale to capture such events.<sup>74,75</sup> Altogether, these results suggest that the presence of a small molecule probe may in some cases not be able to induce fully conformational change, especially in small time scales within 20 ns each. A longer time scale or a larger scaffold (such as the indolin-2-one building block of compound 2) may be necessary to obtain the desired conformation. However, utilizing larger chemical probes also increases the likelihood of phase separation, resulting in inefficient mapping. Therefore, optimization of the concentration and parameters of the chemical probes is warranted.

**Interleukin-36 $\gamma$ .** IL-36 $\gamma$  is another test case we included in this study. This cytokine is the eighth member of the IL-1 family and plays an important role in the pathogenesis of psoriasis. A-552 was discovered as an effective small-molecule antagonist of IL-36 $\gamma$  following a comprehensive high-throughput screening conducted by AbbVie.<sup>26</sup> This ligand blocks the interaction between IL-36 $\gamma$  and its receptor complex, IL-36R/IL-1R $\alpha$ C $\beta$ , as demonstrated by TR-FRET measurements and functional assays on cells secreting IL-8 upon IL-36 $\gamma$  stimulation. Notably, this compound selectively targets IL-36 $\gamma$  and not other cytokines in the IL-36 subfamily. It has shown efficacy in attenuating IL-36 $\gamma$ -induced responses in both murine and human plaque psoriasis models. A-552 binds directly to IL-36 $\gamma$  with high affinity, engaging a cryptic pocket that is not exposed in the apo structure.<sup>26</sup> This binding process involves conformational shifts in the backbone of the C-terminal segment (Leu165–Asp169) and the side chains of residues Asp121, Lys123, and Leu165 with migration angles of approximately 58.5, 60.1, and 84.6 degrees, respectively (Figure 3A). These alterations facilitate the formation of a pocket that effectively accommodates A-552. Figure 3B illustrates the mapping of the ligand A-552 onto the apo form of IL-36 $\gamma$ . Such a cryptic site on the apo structure poses an enormous challenge to conventional binding site prediction tools.

For comparison purposes with MixMD, we also utilized FTMap, a binding hotspot mapping server via various probe molecules docking, energy minimization, and clustering based on average free energy.<sup>74</sup> Among the various mapped sites (Figure S4A), a small pocket near the position of A-552 on the apo IL-36 $\gamma$  was detected by FTMap. Using FTSite<sup>75</sup> to rank binding hotspots by the number of nonbonded contacts, this site ranked second among the three discovered pockets (Figure S4B). However, this pocket only overlaps with a small part of A-552, specifically in the methylpyrimidine group.

When applying MixMD to the apo structure of IL-36 $\gamma$ , the position of the A-552 ligand was detected and mapped well to

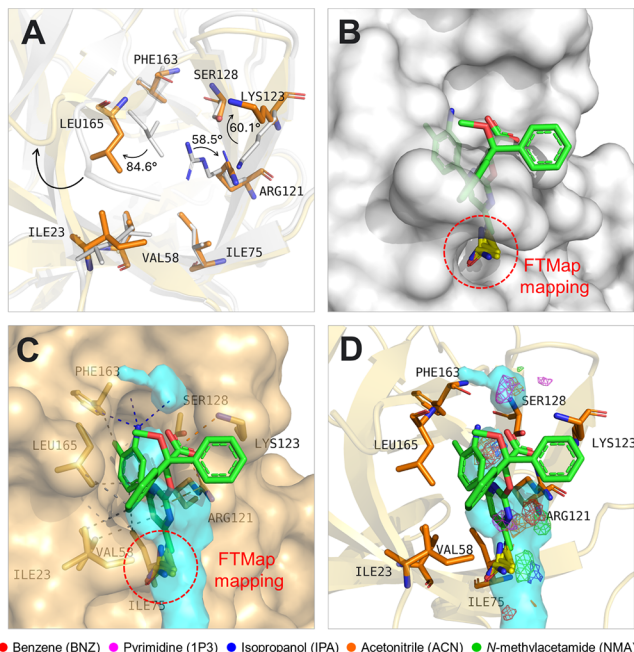


**Figure 3.** (A) Superimposition of IL-36 $\gamma$  in apo conformation (white: PDB 4IZE) and holo conformation (orange: PDB 6P9E). (B) The overlay of A-552 on the surface of IL-36 $\gamma$  reveals that the cryptic pocket is not evident in the unbound form. (C,D) MixMD mappings on the surface of IL-36 $\gamma$  suggest that MixMD could capture the opening of the cryptic site and map the core scaffold of an ideal inhibitor. Mesh representatives (at  $z = 20\sigma$ ) in different colors indicate different mappings of the probes while the cyan surface represents the clustering results of MixMD ProbeView.

the open binding pocket in the holo-structure (Figure 3C). The probe molecules also map better than FTMap onto the structural regions of the ligand (Figure 3D). First, BNZ correctly mapped the positions of the methylpyrimidine and methylaniline rings of A-552. A hotspot identified by 1P3 also appears adjacent to the methylpyrimidine group. Non-absolutely, ACN, NMA, and IPA are representative probe molecules for hydrogen bonding capacity mapped in the vicinity of heterocyclic nitrogen atoms or amino groups of A-552. The biphenyl group of the ligand was not mapped by any hotspot. This is reasonable since the biphenyl group does not interact with any residues in the holo-structure, but it only plays a role in hindering the access of IL-36R to IL-36 $\gamma$ , as explained by Todorović et al.<sup>26</sup>

**Hot-Spot Mapping and Automated Site Prediction on IL-33 Using MixMD.** The results presented above demonstrate the effectiveness of MixMD in identifying experimental binding sites on IL-1 family cytokines. Following this success, we applied the same protocol to the crystal structure of IL-33 (PDB 4KC3) to investigate the existence of similar binding cavities that are present in other members of its family.

Figure 4A highlights the delineated hotspots on IL-33 at  $z = 20\sigma$ . First, our analysis revealed that probe molecules exhibited a higher occupancy on IL-33 compared to IL-1 $\beta$  and IL-36 $\gamma$  (Figure S5). Therefore, we set a cutoff of 0.2 for the DBSCAN clustering algorithm in the MixMD Probeview program. This adjustment allowed for the identification and visualization of the top 10 binding cavities (Figure 4B). These sites were ranked according to their size and probe occupancy levels (see Table S4). Notably, BNZ (red), ACN (orange), and NMA

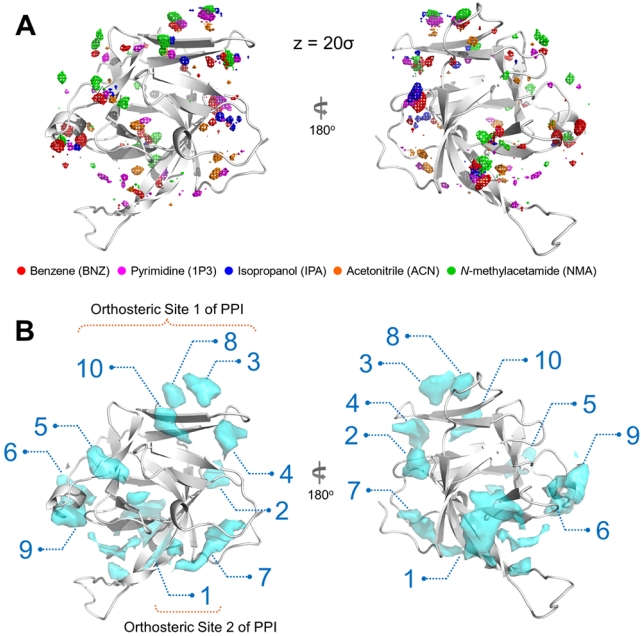


**Figure 4.** (A) Hotspots mapped on IL-33 using five aqueous miscible chemical probes at  $z = 20\sigma$ . Mesh representatives in different colors indicate different mappings of the probes. (B) Ten predicted binding sites as cyan surfaces using the clustering algorithm of MixMD ProbeView.

(green) exhibit the most significant occupancies on the protein surface, exceeding those of IPA (blue) and 1P3 (purple). This observation further emphasizes the cytokine's highly lipophilic characteristics and its capability to interact with the amide linkage in NMA (a common pattern in PPIs) and BNZ (a common scaffold that represents aromatic and hydrophobic features).

Our MixMD simulations revealed that both the PPI orthosteric sites between IL-33 and ST2 attracted the interactions of probe molecules. In particular, Site 1 was identified with three distinct subpockets (ranked 3, 8, and 10). This result suggests that focusing on a potential binding pocket may provide better ligand binding efficiency than using the entire PPI interface. Conversely, orthosteric Site 2 corresponded to a single and highest-ranked cavity, highlighting its greater potential for ligand binding. Figure 4A illustrates that this cavity was occupied by various types of organic probes with high frequency while Figure 5 focuses on each of the detected binding cavities. The fragments that have been found to bind to IL-1 $\beta$  were also superimposed to the structure of IL-33 when relevant in purple (Figure 5A,C).

In a previous study on PPIs between IL-33 and ST2,<sup>6</sup> it was observed that the acidic residues of IL-33 act as hydrogen bond acceptors from the basic residues of the ST2 receptor. This observation aligns with the favorable mapping of the NMA probe on both interacting interfaces. Furthermore, the binding hotspots of BNZ and 1P3 corresponded to the positions of aromatic residues at Site 1, including Tyr129, Asn130, Glu139, Tyr146, Asp149, and Leu150 reflecting their interactions with Tyr132, Phe20, Pro37, and Tyr119 of the ST2 receptor (Figure 5A). This pattern is also mirrored at Site 2 (Figure 5B) where probe molecules aligned with Tyr163, Leu182, Val228, and Leu267 corresponding to interactions with Leu246, Leu306, Leu308, and Phe245 of ST2. Intriguingly at both orthosteric sites, the aromatic probes were capable of

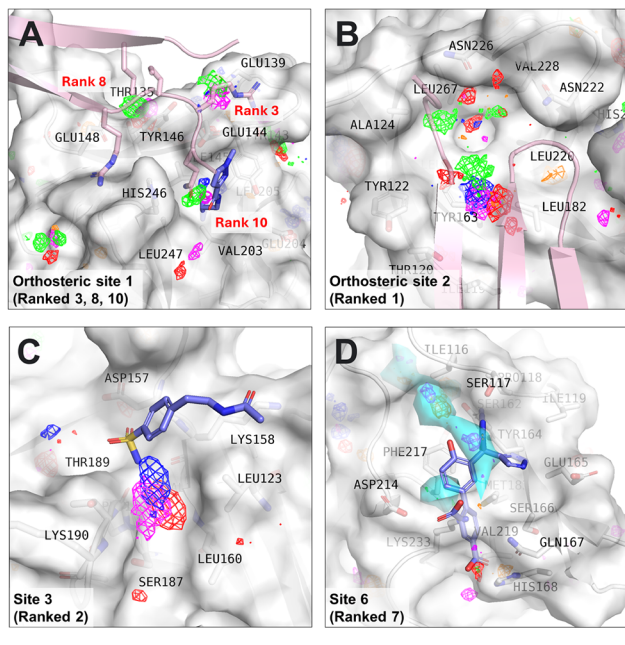


**Figure 5.** Selected potential binding sites were captured by MixMD (at  $z = 20\sigma$ ) on the surface of IL-33. The light pink representation illustrates the protein residues from the ST2 receptor, text annotations indicate the IL-33 residues delineating the binding sites, and the cyan surface represents the results from MixMD ProbeView. IL-1 $\beta$  binders (purple sticks) are superimposed on the surface of IL-33 to demonstrate the druggability potential of these binding sites. (A) Three smaller binding sites were identified on orthosteric site 1, and the site ranked 10 aligns with site 2 of IL-1 $\beta$ . (B) Orthosteric site 2 is the largest detected binding site on IL-33, mirroring the side chains of ST2. Aromatic probes penetrated the surface of IL-33, indicating the opening of cryptic pockets not observed in the crystal structure. (C) Site 3 is a small groove mapped by three out of five probes, coinciding with site 3 of IL-1 $\beta$ . (D) Site 6 is a cryptic site positioned similarly to site 4 from IL-1 $\beta$ . Compound 2 by Hommel et al.<sup>25</sup> is shown for reference to the location of this site.<sup>6,25</sup>

penetrating the surface of IL-33 and collapsed with the protein side chain similar to observations in IL-36 $\gamma$ . This observation suggests that aromatic moieties in organic compounds may induce the rearrangement of proximal side chains to form cryptic pockets thereby enhancing binding affinity with IL-33. Regarding polar interactions, the predominant mapping of probe molecules to the hotspot residues, Lys22, Arg35, Gln39, and Arg38 of ST2 underscores the critical role of these residues at Site 1 in facilitating complex formation with IL-33.

Significantly, a cavity ranked 7 was identified near the N-terminus and the  $\beta$ 8– $\beta$ 9 loop of IL-33, mapped by 1P3 and ACN probes. Furthermore, when considering an adjacent area mapped by BNZ and 1P3 (Figure 5D), these regions together could potentially constitute a binding pocket closely resembling the cryptic pocket of the ligand 2 on IL-1 $\beta$ . Although MixMD did not reveal such a cryptic pocket on IL-33 using only small probes – a finding consistent with previous observations on IL-1 $\beta$  – the current results suggest the possible formation of a cryptic site when induced by a suitable ligand.

**A Known Inhibitor May Bind to IL-33 Mainly via Nonspecific Hydrophobic Interactions.** In 2016, Kim et al. reported BTB11086 (2-phenyl-SH-[1,3]oxazolo[4,5-*c*]-quinoline-4-one) as a selective binder to the hydrophobic

interface of IL-33 (referred to as Site 2 in this study).<sup>20</sup> Subsequently, the same group synthesized a series of compounds based on the oxazolo[4,5-*c*]-quinolinone scaffold, among which compound 7c emerged as the most potent inhibitor against IL-33.<sup>19</sup> Follow-up NMR binding studies suggested that compound 7c shares the same binding pocket as BTB11086. However, the detailed atomistic mechanism underlying the inhibition of IL-33 by these compounds remained elusive. Therefore, in this study, we conducted five independent 1-microsecond MD simulations to elucidate the atomistic mechanism of action of compound 7c.

Figure 6A illustrates the interaction fingerprints between 7c and IL-33 throughout the MD trajectories, showing only the prominent interactions (sparse and rare interactions are omitted). Long time scale simulations revealed multiple binding patterns and interactions between 7c and IL-33. Hydrophobic interactions and *van der Waals* contacts emerged as the primary driving forces for the binding of 7c to IL-33. Tyr163 exhibited the highest interaction frequency, participating in numerous hydrophobic, *van der Waals*, and  $\pi$ – $\pi$  interactions. Furthermore, the binding of 7c was supported by hydrophobic interactions with residues Ile119, Thr120, Leu182, Leu220, and Leu267. In addition to hydrophobic forces, electrostatic interactions such as  $\pi$ –cation interactions and hydrogen bonds likely contributed to the binding of 7c. In several trajectories, the tertiary amine group of 7c formed a  $\pi$ –cation interaction with the side chain of Tyr122, while Asn222 potentially formed up to two hydrogen bonds with 7c simultaneously.

MD simulations generated a plethora of binding conformations of 7c within the desired binding pocket, necessitating clustering to identify the most prevalent binding poses. More than 20 clusters were identified, with the five most frequent ones, accounting for approximately 62% of the frames, being presented in Figure 6B–F.

Cluster 1 represents the most frequently observed binding pose of 7c, accounting for 21.82% of the frames. In this cluster, the trifluorophenyl ring is deeply inserted into the cryptic hydrophobic groove, surrounded by Leu161 and Leu267, facilitating hydrophobic interactions with the hydrophobic core composed of Leu126 and Phe230. The formation of this binding groove required the movement of Leu267 and Asn226, opening the entrance for small molecules to interact with the hydrophobic core. Figure S6 illustrates the closed and open states of the cryptic pocket to elucidate the structural changes that occur upon ligand binding. The presence of a cryptic site has been suggested by several BNZ mapping (red) in the center of this groove (Figure 6B), indicating the effectiveness of MixMD in mapping unpredictable cryptic pockets. The oxazolo[4,5-*c*]-quinolinone ring of the ligand engaged in  $\pi$ – $\pi$  interactions with Tyr163 and hydrophobic contacts with adjacent residues, including Ile119, Thr120, Tyr122, Leu182, and Leu220. Additionally, the heteroatom N of the oxazole ring or the O atom of the alkoxy side chain contributed to two hydrogen bonds with Asn222. The ammonium alkoxy chain formed another hydrogen bond with Asp175, potentially stabilizing the structure and rendering it unfavorable for binding with the ST2 receptor.

The protein conformation of IL-33 in Cluster 2 closely resembled that of Cluster 1, exhibiting an opened cryptic pocket not apparent in the initial crystal structure (Figure 6C). The main difference lies in the orientation of the three-ring system, perpendicular to the plane in Cluster 2 and enabling



**Figure 6.** (A) Protein–ligand interaction fingerprints between IL-33 and compound 7c along the five independent 1- $\mu$ s MD simulations using the ProLIF program. (B–F) Representative poses of the most abundant ligand conformations during the simulations were extracted using the Quality Threshold Clustering algorithm based on the ligand heavy atoms. Cluster 1 is the most abundant and most likely pose that represents the inhibitory mechanism of 7c. For further information refer to the text.

the interactions with the hydrophobic core, while the trifluorophenyl ring stacks with Tyr163. Despite the interchangeability of the two ring systems due to unspecific hydrophobic interactions, results from MM-GBSA  $\Delta G_{bind}$  estimations, and ligand fitness to the binding pocket, along with pose abundance, favor the binding pose of Cluster 1 over Cluster 2.

Clusters 3 and 4 exhibit highly similar conformations of the ligand, characterized by the trifluorophenyl ring positioned similarly to  $\pi$ – $\pi$  stack with Tyr163, and the three-ring system engaging in  $\pi$ – $\pi$  stacking with Tyr122 (Figure 6D,E). However, a notable distinction arises in the orientation of the alkoxy side chain. In Cluster 3, the ammonium group points toward the C-terminal Thr270, forming a salt bridge with this residue, whereas in Cluster 4, the side chain orients toward Glu121. However, it should be noted that the estimated  $\Delta G_{bind}$  of these clusters is not as favorable as the previously reported ones. Moreover, the ligand in these clusters binds parallel to the protein surface, lacking anchorage by any residue side chain to prevent dissociation from the binding pocket. This observation suggests a lower likelihood of contributing to the ligand's inhibitory mechanism, indicating reduced affinity or efficacy compared to other binding poses.

Cluster 5, although less abundant than previously reported clusters, is included for its resemblance to the initial docking pose, providing insight into ligand-protein conformational adaptation. In this cluster, the three-ring system aligns parallel to the protein surface, covering the entrance of the previously cryptic pocket, while the trifluorophenyl scaffold engages in  $\pi$ – $\pi$  stacking with Tyr163, akin to Clusters 2–4. The ammonium alkoxy side chain forms both a salt bridge with Glu269 and an  $\pi$ -cation interaction with the aromatic ring of Tyr122, potentially explaining its relatively low  $\Delta G_{bind}$  of -29.67 kcal/mol. Nevertheless, this binding pose is not as preferable as the ones in Clusters 1 and 2, owing to its limited penetration to the protein surface, similar to the case of Clusters 3 and 4.

**The Opening of Cryptic Sites Enhances the Druggability of IL-33 – Suggestion from Multiple Molecular Modeling Techniques.** The more favorable binding free energy and the high frequency of the binding pose in Cluster 1 suggest that this pose likely represents the binding mode of 7c in IL-33. Two questions arise upon the interpretation of the simulation results: (1) whether different molecular docking programs, specifically their scoring functions, would consider our reported binding mode of 7c the most favorable, and (2)

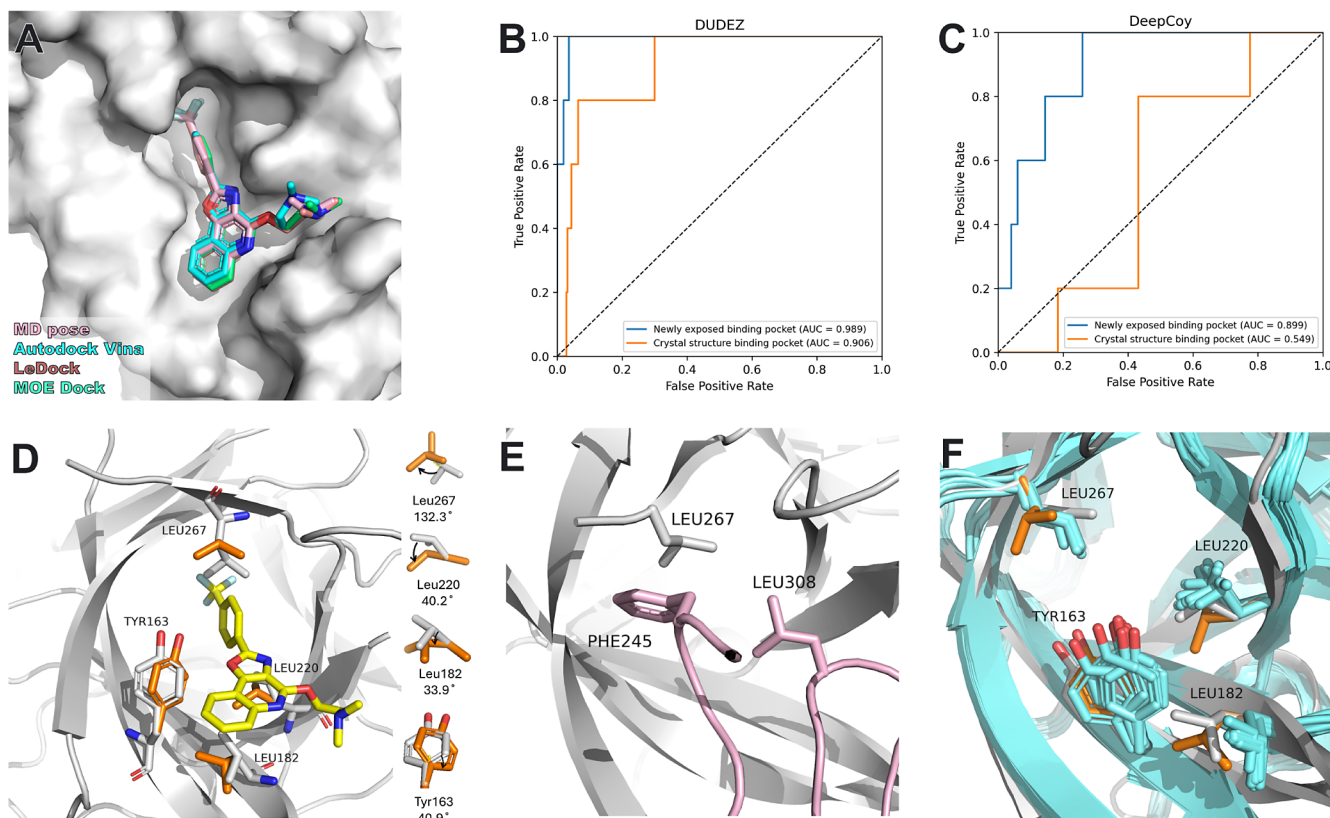


**Figure 7.** (A) Superimposition of the redocked pose and MD pose of **7c** using different docking programs (AutoDock Vina: cyan; LeDock: orange; MOE Dock: light green). (B–C) ROC curve obtained from the docking of 5 actives and 250 decoys retrieved from DUDE-Z server (B) or DeepCoy program (C). (D) Superimposition of the flexible side chains required for the binding of **7c** predicted from the flexible docking algorithm of AutoDock Vina; (E) The orientation of IL-33<sub>Leu267</sub> is blocked by the steric hindrance of ST2<sub>Phe245,Leu308</sub> (PDB ID: 4KC3); (F) Conformations of binding site residues from NMR structure (PDB 2KLL – cyan) in alignment with the residues from crystal structure (white) and from flexible docking suggestion (orange).

whether this binding pocket is preferable for enriching active compounds over inactive ones compared to the crystal structure. To address these questions, we implemented redocking using different molecular docking programs to identify if different scoring functions would produce a comparable binding pose to our proposed pose. Furthermore, we evaluated the capability of this binding pocket to discriminate between actives and presumably decoys from two different decoy generation approaches. These two approaches are commonly used to retrospectively validate a docking protocol before using it for virtual screening purposes.<sup>76,77</sup>

As for the redocking stage, three molecular docking programs were chosen in our study: Autodock Vina, LeDock, and the docking module of MOE (referred to as MOE Dock). These docking programs were selected to represent a wide variety of ligand conformation sampling techniques and scoring functions. As shown in Figure 7A, all docking programs produced comparable binding poses of **7c** in the binding pocket, with the RMSD to the MD pose below 1 Å. The consensus among different algorithms suggests that **7c** likely binds to IL-33 in the same manner as our proposed binding pattern. However, experimental structural evidence is still required to confirm our hypothesis.

To examine the enrichment capabilities of this binding pose, we compared the receiver-operating characteristics (ROC) curve of two docking models using our proposed binding pocket and that of the crystal structure. The same Autodock

Vina parameters were used between the two models. For a more comprehensive and unbiased understanding, we employed two programs, namely DUDE-Z<sup>78</sup> and DeepCoy<sup>79</sup> for the generation of 250 property-matched decoys from the set of 5 actives reported by Kim et al.<sup>19</sup> The results from Figure 7B,C show that the docking model based on our proposed pocket outperformed that of the crystal structure in both cases. The difference in the case of DUDE-Z is not as pronounced as in the case of DeepCoy, suggesting that the deep-learning model was more effective in generating more challenging and harder-to-discriminate decoys. However, our proposed binding pocket was also able to enrich the hits in such challenging tasks. These results suggest that the proposed binding pocket if used in a structure-based drug design or a virtual screening campaign, could be more applicable in detecting active compounds compared to the binding pocket defined in the crystal structure.

For further insight, we also investigated whether a similar binding pose of **7c** could be retrieved from the initial crystal structure when considering the flexibility of the protein's side chains. Therefore, we implemented flexible docking using Autodock Vina, with all the side chains of the residues forming the binding sites being regarded as flexible. The result was interesting as we found that only modest movement of the hydrophobic residues Tyr163, Leu182, Leu220, and Leu267 could afford a similar binding pose of **7c** as retrieved from MD simulations (Figure 7D). The main driver of the binding is the formation of the cryptic binding pocket for the accommoda-

tion of the trifluorophenyl substituent, which is highly dependent on the spatial location of Leu267.

We continued to examine the two experimental protein structures (PDB 4KC3<sup>6</sup> and 2KLL<sup>80</sup>) to discover whether the movement of this residue is evidenced experimentally or hindered by any effects. Unfortunately, in all available structures, the side chain of Leu267 does not tend to orient toward the solvent, hence not showing the proposed binding pocket. We believe that in nature, this side chain is still flexible to a certain extent, but this phenomenon is not captured in the available structures. Regarding the IL-33/ST2 crystal structure (Figure 7E), the flexibility of Leu267 is sterically hindered by the presence of its two interacting residues Phe245 and Leu308 from ST2. This structure has shown a strong conformational selection response of IL-33 toward its receptor, therefore relying solely on this structure could result in potential bias and may not represent the structure of IL-33. Considering the NMR structure of IL-33 in solution (Figure 7F) although the authors resolved up to 100 structures, only the 10 lowest-energy structures were reported, none of which exposed the cryptic pocket.<sup>80</sup> It is important to note that the limited side chain conformational variability of Leu267 in these conformers may be related to the experimental restraints rather than solely reflecting inherent flexibility. We believe that this binding pocket is revealed only in the presence of an organic probe or a small molecule, such as 7c, which can occupy the hydrophobic groove and stabilize the conformation.

## DISCUSSION

To date, IL-33 remains the newest member of the IL-1 subfamily. Inhibiting the PPI between IL-33 and its ST2 receptor emerges as a promising therapeutic strategy for inflammatory, allergic, and autoimmune diseases.<sup>12–15</sup> Until recently, several first-in-class antagonists of related interleukins (IL-1 $\beta$  and IL-36 $\gamma$ ) have been reported, hinting at the feasibility of targeting IL-33 using a small-molecule approach.

We initially employed the MixMD protocol on IL-1 $\beta$  and IL-36 $\gamma$  as retrospective examples to assess its capability of capturing known binding sites. Subsequently, we applied the same protocol to IL-33 to identify potential starting points for structure-based drug design. The MixMD results demonstrated successful mapping of the cryptic binding site of A-552 in IL-36 $\gamma$  and three out of four known binding sites of IL-1 $\beta$ . However, for IL-1 $\beta$ , the protocol only captured the exposed part of the cryptic pocket of an allosteric inhibitor, possibly due to the short simulation time scale. Although attempts to enhance sampling using aMD were made,<sup>81</sup> achieving the desired conformer remained challenging. Nevertheless, our MixMD results effectively detected experimentally reported binding sites and suggested growing directions for enhanced affinity.<sup>73</sup>

Based on the aforementioned success, we applied and identified several putative binding sites on the surface of IL-33, with the most promising site aligning with the hydrophobic interface with ST2. Additionally, we aimed to elucidate the atomistic mechanism of the reported inhibitor 7c, using long time scale, unbiased MD simulations. Protein–ligand interaction fingerprints extracted from MD trajectories revealed that hydrophobic interactions were the primary drivers of compound 7c, binding with polar contacts contributing minimally. Clustering based on heavy atoms of the inhibitor identified two prominent binding poses that aligned well with

MixMD mappings and explained experimental results from NMR chemical shift perturbation studies by Kim et al.<sup>19</sup>

Previously, 7c was reported to induce a noticeable change in HSQC (Heteronuclear Single Quantum Coherence) spectrum of IL-33 in ten residues of the IL-33/ST-2 interface (residues 120, 121, 161, 220, 224, 226, 227, 229, 267, and 269) and two amino acids in the hydrophobic core (residues 184 and 185). Figure 8A illustrates the overlay of these residues in the crystal

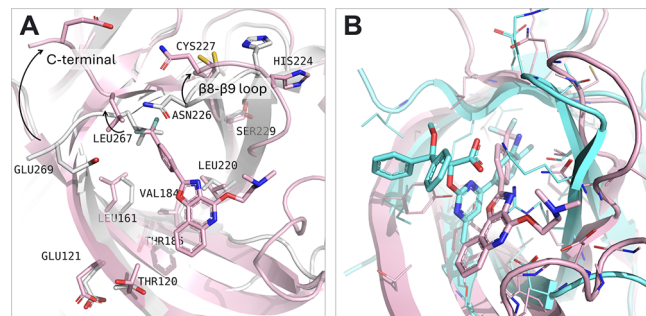


**Figure 8.** (A) The overlay of the residues that were reported to be perturbed in NMR CSP experiments between the crystal structure (white) and the structure in complex with 7c during MD simulations (pink); (B) The overlay of the suggested binding pose of 7c in IL-33 (pink) and the binding pose of A-552 in IL-36 $\gamma$  (cyan) – the corresponding protein residues are plotted as line representation and in the same color.

conformation and that in the complex with our proposed binding pose in Cluster 1. As we already mentioned previously, the binding of 7c requires the rearrangement of the C-terminal (residues 267–270) and the  $\beta$ 8– $\beta$ 9 loop (residues 221–229) to make room for the trifluorophenyl scaffold of the compound. The opening of this cryptic hydrophobic groove also exposed the side chain of Leu161, Val184, and Leu220 which could better explain the mechanism of perturbation of these residues upon the binding of 7c, in comparison with the hypothesis proposed by Kim et al. in the same report. We assume that the formation or opening of this cryptic pocket is the key factor for the stable binding of compound 7c and could explain its inhibitory mechanism. However, it is important to note that this binding cluster is still not able to explain the CSP of Glu121 and Thr120 as the backbone of these residues remained relatively unchanged between the two conformations.

More intriguingly, upon alignment with the IL-36/A-552 complex, we found a surprisingly great agreement between our proposed binding pose with that of A-552 (Figure 8B). In both complexes, the aromatic scaffold of the compounds penetrates deeply into the hydrophobic groove of the protein, forming additional hydrophobic interactions with deeply buried side chains to form a more stable complex. On the other hand, the outward side of the compounds tends to form additional hydrophilic or hydrophobic interactions with the adjacent residues. This notion further underscores the importance of cryptic pockets in IL-33 as potential binding sites for inhibitors. However, further experimental validation is necessary to confirm this hypothesis.

Despite recent advances in pharmaceutical science, designing drugs that target PPIs remains a formidable challenge, largely due to the flat, featureless, and widespread nature of PPI surfaces. Druggability assessment and target validation are thus pivotal to avoid wasting time and resources on

undruggable targets. Computational methods have emerged as effective tools for assessing druggability once the 3D structure of the protein is available.<sup>8,2</sup> However, cryptic sites, which are not evident in the apo structure, add complexity, as they are only revealed when considering protein–ligand interactions and side chain flexibility, aspects often overlooked in static crystal structures. MixMD has emerged as a solution to this challenge by enabling protein interaction with the environment and organic probes, mimicking the binding of small molecules in nature. Research on the IL-1 subfamily so far has shown that antagonists may target cryptic sites, suggesting a similar phenomenon in the case of IL-33. Our proposed binding pockets exhibit a strong induced-fit effect, with multiple favorable interactions between the ligand and protein. These conformations likely better reflect real-life binding events than crystal structures and could serve as templates for subsequent structure-based drug design efforts. The protein structures corresponding to these binding modes are available as *Supporting Materials*, which could be used for further exploration and development.

## CONCLUSIONS

IL-33, the newest member of the IL-1 family, exerts its biological function through interaction with the ST2 receptor. Inhibiting the IL-33/ST2 PPI has shown therapeutic promise in various diseases, including allergy, inflammation, and autoimmunity. Traditionally, it was assumed that targeting this PPI directly by binding to either of the two interfaces would suffice, without systematic assessment of its druggability or exploration of alternative binding sites.

In this study, we employed MixMD simulations to identify putative binding pockets on the IL-33 protein. Initially, we validated the protocol by applying MixMD simulations to IL-1 $\beta$  and IL-36 $\gamma$ , two other IL-1 family members with known binding sites. The results demonstrated that MixMD could detect most binding pockets, including cryptic ones not evident in the input crystal structure. This capability distinguishes MixMD from other binding site detection methods reliant solely on static protein structures such as FTMap. Subsequently, we applied the same method to IL-33, identifying ten binding hotspots corresponding to both orthosteric (IL-33/ST2 interfaces) and potential allosteric sites. It is important to note that we refer to the latter as potential allosteric sites pending further evidence regarding their biological activity.

Further investigation focused on the most promising binding sites on IL-33, aligned with Site 2 reported by Liu et al.<sup>6</sup> Five long time scale MD simulations were conducted to elucidate the binding pattern of 7c in this pocket. Clustering of the ligand pose during the trajectories revealed intriguing induced-fit effects of IL-33 toward 7c, indicating a cryptic pocket not evident in the crystal structure of the IL-33/ST2 complex. Results from multiple molecular modeling methods further support the existence of this cryptic binding site. Additionally, our proposed binding patterns offer better explanations for IL-33 CSP experiment results upon 7c binding compared to docking results from Kim et al.<sup>19</sup>

In conclusion, our study has unveiled several potential binding sites on the surface of IL-33 and suggested the presence of a cryptic pocket in the second interface between IL-33 and ST2, which is more druggable and accessible for targeting. These findings could expedite the discovery of small molecule modulators for IL-33.

## ASSOCIATED CONTENT

### SI Supporting Information

The Supporting Information is available free of charge at <https://pubs.acs.org/doi/10.1021/acs.jpcb.4c03057>.

Available PDB structures of 11 IL-1 family members, benzene (BNZ) parameters for MixMD, the ratio of organic solvent and water molecule in 5% v/v MixMD systems, occupancy of each probe molecule and the total occupancy in the top ten clusters (binding sites) of IL-33 identified by MixMD Probeview, docking parameters for IL-33, MixMD mapping results applied on IL-1 $\beta$  at 10 $\sigma$ , and binding hotspots mapped by FTSuite on the apo structure of IL-36 $\gamma$  ([PDF](#))

The prepared protein structures of IL-1 $\beta$  (PDB), IL-36 $\gamma$  (PDB), and IL-33; the proposed binding modes of 7c in complex with IL-33 during the MD simulations; the PyMOL session indicating the detected binding sites on IL-33; the modified Python 3 version of MixMD ProbeView ([ZIP](#))

## AUTHOR INFORMATION

### Corresponding Author

Khac-Minh Thai – Department of Medicinal Chemistry, Faculty of Pharmacy, University of Medicine and Pharmacy at Ho Chi Minh City, Ho Chi Minh City 700000, Vietnam; [orcid.org/0000-0002-5279-9614](https://orcid.org/0000-0002-5279-9614); Phone: (+84) 909 680 385; Email: [thaikhacminh@gmail.com](mailto:thaikhacminh@gmail.com)

### Authors

Tan Thanh Mai – Department of Medicinal Chemistry, Faculty of Pharmacy, University of Medicine and Pharmacy at Ho Chi Minh City, Ho Chi Minh City 700000, Vietnam; [orcid.org/0000-0001-7313-9853](https://orcid.org/0000-0001-7313-9853)

Thua-Phong Lam – Department of Medicinal Chemistry, Faculty of Pharmacy, University of Medicine and Pharmacy at Ho Chi Minh City, Ho Chi Minh City 700000, Vietnam; Department of Cell and Molecular Biology, Uppsala University, Uppsala 75124, Sweden; [orcid.org/0000-0002-8149-9952](https://orcid.org/0000-0002-8149-9952)

Long-Hung Dinh Pham – Department of Medicinal Chemistry, Faculty of Pharmacy, University of Medicine and Pharmacy at Ho Chi Minh City, Ho Chi Minh City 700000, Vietnam; Department of Chemistry, Imperial College London, London W12 0BZ, United Kingdom

Kim-Hung Nguyen – Department of Biochemistry, Faculty of Pharmacy, University of Medicine and Pharmacy at Ho Chi Minh City, Ho Chi Minh City 700000, Vietnam

Quoc-Thai Nguyen – Department of Biochemistry, Faculty of Pharmacy, University of Medicine and Pharmacy at Ho Chi Minh City, Ho Chi Minh City 700000, Vietnam

Minh-Tri Le – Department of Medicinal Chemistry, Faculty of Pharmacy, University of Medicine and Pharmacy at Ho Chi Minh City, Ho Chi Minh City 700000, Vietnam; University of Health Sciences, Vietnam National University Ho Chi Minh City, Ho Chi Minh City 700000, Vietnam; Research Center for Discovery and Development of Healthcare Products, Vietnam National University Ho Chi Minh City, Ho Chi Minh City 700000, Vietnam

Complete contact information is available at:

<https://pubs.acs.org/doi/10.1021/acs.jpcb.4c03057>

**Notes**

The authors declare no competing financial interest.

**ACKNOWLEDGMENTS**

This research was funded by the University of Medicine and Pharmacy at Ho Chi Minh City grant number 224/2022/HĐ-HYD for Khac-Minh Thai. Tan Thanh Mai was funded by Vingroup Joint Stock Company and supported by the Domestic Master/PhD Scholarship Programme of Vingroup Innovation Foundation (VINIF) Vingroup Big Data Institute (VINBIGDATA) code VINIF.2019.TS.59 and VINIF.2020.TS.128.

**ABBREVIATIONS**

IL;interleukin; CSP;chemical shift perturbation; HSQC;heteronuclear single quantum coherence; MD;molecular dynamics; MixMD;mixed-solvent molecular dynamics; PPI;protein–protein interaction; TR-FRET;time-resolved fluorescence resonance energy transfer

**REFERENCES**

- (1) Akdis, M.; Burgler, S.; Crameri, R.; Eiwegger, T.; Fujita, H.; Gomez, E.; Klunker, S.; Meyer, N.; O'Mahony, L.; Palomares, O.; et al. Interleukins from 1 to 37 and interferon-gamma: Receptors functions and roles in diseases. *J. Allergy Clin. Immunol.* **2011**, *127* (3), 701–721.
- (2) Schmitz, J.; Owyang, A.; Oldham, E.; Song, Y.; Murphy, E.; McClanahan, T. K.; Zurawski, G.; Moshrefi, M.; Qin, J.; Li, X.; et al. IL-33 an interleukin-1-like cytokine that signals via the IL-1 receptor-related protein ST2 and induces T helper type 2-associated cytokines. *Immunity* **2005**, *23* (5), 479–490.
- (3) Cayrol, C.; Girard, J.-P. Interleukin-33 (IL-33): A critical review of its biology and the mechanisms involved in its release as a potent extracellular cytokine. *Cytokine* **2022**, *156*, 155891.
- (4) Liew, F. Y.; Girard, J.-P.; Turnquist, H. R. Interleukin-33 in health and disease. *Nat. Rev. Immunol.* **2016**, *16* (11), 676–689.
- (5) Griesenauer, B.; Paczesny, S. The ST2/IL-33 Axis in Immune Cells during Inflammatory Diseases. *Front. Immunol.* **2017**, *8*, 475.
- (6) Liu, X.; Hammel, M.; He, Y.; Tainer, J. A.; Jeng, U. S.; Zhang, L.; Wang, S.; Wang, X. Structural insights into the interaction of IL-33 with its receptors. *Proc. Natl. Acad. Sci. U. S. A.* **2013**, *110* (37), 14918–14923.
- (7) Gorbacheva, A. M.; Mitkin, N. A. Interleukin-33: Friend or Enemy in the Fight against Tumors? *Mol. Biol.* **2019**, *53* (5), 681–695.
- (8) Liang, Y.; Ge, Y.; Sun, J. IL-33 in COVID-19: Friend or foe? *Cell. Mol. Immunol.* **2021**, *18* (6), 1602–1604.
- (9) Zhang, J.; Ramadan, A. M.; Griesenauer, B.; Li, W.; Turner, M. J.; Liu, C.; Kapur, R.; Hanenberg, H.; Blazar, B. R.; Tawara, I.; et al. ST2 blockade reduces sST2-producing T cells while maintaining protective mST2-expressing T cells during graft-versus-host disease. *Sci. Transl. Med.* **2015**, *7* (308), 308ra160.
- (10) Ramadan, A.; Land, W. G.; Paczesny, S. Editorial: Danger Signals Triggering Immune Response and Inflammation. *Front. Immunol.* **2017**, *8*, 979.
- (11) Van der Jeught, K.; Sun, Y.; Fang, Y.; Zhou, Z.; Jiang, H.; Yu, T.; Yang, J.; Kamocka, M. M.; So, K. M.; Li, Y.; et al. ST2 as checkpoint target for colorectal cancer immunotherapy. *JCI Insight* **2020**, *5* (9), No. e136073.
- (12) Okragly, A. J.; Corwin, K. B.; Elia, M.; He, D.; Schroeder, O.; Zhang, Q.; Shyanova, T.; Bright, S.; Dicker, S. B.; Chlewnicki, L.; et al. Generation and Characterization of Torudokimab (LY3375880): A Monoclonal Antibody That Neutralizes Interleukin-33. *J. Inflammation Res.* **2021**, *14*, 3823–3835.
- (13) Chen, Y. -L.; Gutowska-Owiak, D.; Hardman, C. S.; Westmoreland, M.; MacKenzie, T.; Cifuentes, L.; Waithe, D.; Lloyd-Lavery, A.; Marquette, A.; Londei, M.; et al. Proof-of-concept clinical trial of etokimab shows a key role for IL-33 in atopic dermatitis pathogenesis. *Sci. Transl. Med.* **2019**, *11* (515), No. eaax2945.
- (14) Wechsler, M. E.; Ruddy, M. K.; Pavord, I. D.; Israel, E.; Rabe, K. F.; Ford, L. B.; Maspero, J. F.; Abdulai, R. M.; Hu, C.-C.; Martincova, R.; et al. Efficacy and Safety of Itepekimab in Patients with Moderate-to-Severe Asthma. *N. Engl. J. Med.* **2021**, *385* (18), 1656–1668.
- (15) England, E.; Rees, D. G.; Scott, I. C.; Carmen, S.; Chan, D. T. Y.; Chaillan Huntington, C. E.; Houslay, K. F.; Erngren, T.; Penney, M.; Majithiya, J. B.; et al. Tozorakimab (MEDI3506): An anti-IL-33 antibody that inhibits IL-33 signalling via ST2 and RAGE/EGFR to reduce inflammation and epithelial dysfunction. *Sci. Rep.* **2023**, *13* (1), 9825.
- (16) Murphy, A. J.; Papadopoulos, N. J.; Orengo, J. *IL-33 antagonists and uses thereof*. WO2014152195A1. 2014.
- (17) Nguyen, T. T. T.; Truong, T. H. D.; Le, G. B.; Duong, H. X.; Nguyen, Q. B.; Nguyen, D. Q. Generation and characterization of soluble interleukin-33 receptor fused with immunoglobulin gamma-1 constant domain expressed by *Pichia pastoris* yeast. *J. Pharm. Pharmacol.* **2015**, *67* (3), 329–337.
- (18) Nichols, C.; Ng, J.; Keshu, A.; Kelly, G.; Conte, M. R.; Marber, M. S.; Fraternali, F.; De Nicola, G. F. Mining the PDB for Tractable Cases Where X-ray Crystallography Combined with Fragment Screens Can Be Used to Systematically Design Protein–Protein Inhibitors: Two Test Cases Illustrated by IL1 $\beta$ -IL1R and p38 $\alpha$ -TAB1 Complexes. *J. Med. Chem.* **2020**, *63* (14), 7559–7568.
- (19) Kim, Y.; Ma, C.; Park, S.; Shin, Y.; Lee, T.; Paek, J.; Hoon Kim, K.; Jang, G.; Cho, H.; Son, S.; et al. Rational Design Synthesis and Evaluation of Oxazolo [4,5-c]-quinolinone Analogs as Novel Interleukin-33 Inhibitors. *Chem. - Asian J.* **2021**, *16* (22), 3702–3712.
- (20) Kim, Y. K.; Cho, S. H.; Mushtaq, A. U.; Cho, H.; Jung, Y. W.; Byun, Y.; Jeon, Y. H. Discovery of an interleukin 33 inhibitor by molecular docking simulation and NMR Analysis. *Bull. Korean Chem. Soc.* **2016**, *37* (2), 117–118.
- (21) Adamu, R. M.; Singh, R. M.; Ibrahim, M. A.; Uba, A. I. Virtual discovery of a hetero-cyclic compound from the Universal Natural Product Database (UNPD36) as a potential inhibitor of interleukin-33: Molecular docking and dynamic simulations. *J. Biomol. Struct. Dyn.* **2022**, *40* (19), 8696–8705.
- (22) Vinh, L. B.; Han, Y. K.; Park, S. Y.; Kim, Y. J.; Phong, N. V.; Kim, E.; Ahn, B.-G.; Jung, Y. W.; Byun, Y.; Jeon, Y. H.; et al. Identification of triterpenoid saponin inhibitors of interleukin (IL)-33 signaling from the roots of *Astragalus membranaceus*. *J. Funct. Foods* **2023**, *101*, 105418.
- (23) Le, M. T.; Mai, T. T.; Huynh, P. N. H.; Tran, T. D.; Thai, K. M.; Nguyen, Q. T. Structure-based discovery of interleukin-33 inhibitors: A pharmacophore modelling molecular docking and molecular dynamics simulation approach. *SAR QSAR Environ. Res.* **2020**, *31* (12), 883–904.
- (24) Berman, H. M.; Westbrook, J.; Feng, Z.; Gilliland, G.; Bhat, T. N.; Weissig, H.; Shindyalov, I. N.; Bourne, P. E. The Protein Data Bank. *Nucleic Acids Res.* **2000**, *28* (1), 235–242.
- (25) Hommel, U.; Hurth, K.; Rondeau, J.-M.; Vulpetti, A.; Ostermeier, D.; Boettcher, A.; Brady, J. P.; Hediger, M.; Lehmann, S.; Koch, E.; et al. Discovery of a selective and biologically active low-molecular weight antagonist of human interleukin-1 $\beta$ . *Nat. Commun.* **2023**, *14* (1), 5497.
- (26) Todorović, V.; Su, Z.; Putman, C. B.; Kakavas, S. J.; Salte, K. M.; McDonald, H. A.; Wetter, J. B.; Paulsboe, S. E.; Sun, Q.; Gerstein, C. E.; et al. Small Molecule IL-36 $\gamma$  Antagonist as a Novel Therapeutic Approach for Plaque Psoriasis. *Sci. Rep.* **2019**, *9* (1), 9089.
- (27) Liao, J.; Wang, Q.; Wu, F.; Huang, Z. In Silico Methods for Identification of Potential Active Sites of Therapeutic Targets. *Molecules* **2022**, *27* (20), 7103.
- (28) Soga, S.; Shirai, H.; Kobori, M.; Hirayama, N. Use of Amino Acid Composition to Predict Ligand-Binding Sites. *J. Chem. Inf. Model.* **2007**, *47* (2), 400–406.

- (29) Halgren, T. A. Identifying and Characterizing Binding Sites and Assessing Druggability. *J. Chem. Inf. Model.* **2009**, *49* (2), 377–389.
- (30) Le Guilloux, V.; Schmidke, P.; Tuffery, P. Fpocket: An open source platform for ligand pocket detection. *BMC Bioinf.* **2009**, *10* (1), 168.
- (31) Volkamer, A.; Kuhn, D.; Rippmann, F.; Rarey, M. DoGSiteScorer: A web server for automatic binding site prediction analysis and druggability assessment. *Bioinformatics* **2012**, *28* (15), 2074–2075.
- (32) Tian, W.; Chen, C.; Lei, X.; Zhao, J.; Liang, J. CASTP 3.0: Computed atlas of surface topography of proteins. *Nucleic Acids Res.* **2018**, *46* (W1), W363–W367.
- (33) Ravindranath, P. A.; Sanner, M. F. AutoSite: An automated approach for pseudo-ligands prediction—from ligand-binding sites identification to predicting key ligand atoms. *Bioinformatics* **2016**, *32* (20), 3142–3149.
- (34) Kozakov, D.; Grove, L. E.; Hall, D. R.; Bohnuud, T.; Mottarella, S. E.; Luo, L.; Xia, B.; Beglov, D.; Vajda, S. The FTMap family of web servers for determining and characterizing ligand-binding hot spots of proteins. *Nat. Protoc.* **2015**, *10* (5), 733–755.
- (35) Krivák, R.; Hoksza, D. P2Rank: Machine learning based tool for rapid and accurate prediction of ligand binding sites from protein structure. *J. Cheminf.* **2018**, *10* (1), 39.
- (36) Jiménez, J.; Doerr, S.; Martínez-Rosell, G.; Rose, A. S.; De Fabritiis, G. DeepSite: Protein-binding site predictor using 3D-convolutional neural networks. *Bioinformatics* **2017**, *33* (19), 3036–3042.
- (37) Aggarwal, R.; Gupta, A.; Chelur, V.; Jawahar, C. V.; Priyakumar, U. D. DeepPocket: Ligand Binding Site Detection and Segmentation using 3D Convolutional Neural Networks. *J. Chem. Inf. Model.* **2022**, *62* (21), 5069–5079.
- (38) Meller, A.; Ward, M.; Borowsky, J.; Kshirsagar, M.; Lotthammer, J. M.; Oviedo, F.; Ferres, J. L.; Bowman, G. R. Predicting locations of cryptic pockets from single protein structures using the PocketMiner graph neural network. *Nat. Commun.* **2023**, *14* (1), 1177.
- (39) Lexa, K. W.; Carlson, H. A. Full Protein Flexibility Is Essential for Proper Hot-Spot Mapping. *J. Am. Chem. Soc.* **2011**, *133* (2), 200–202.
- (40) Ghanakota, P.; Carlson, H. A. Driving Structure-Based Drug Discovery through Cosolvent Molecular Dynamics. *J. Med. Chem.* **2016**, *59* (23), 10383–10399.
- (41) Ung, P. M. U.; Ghanakota, P.; Graham, S. E.; Lexa, K. W.; Carlson, H. A. Identifying binding hot spots on protein surfaces by mixed-solvent molecular dynamics: HIV-1 protease as a test case. *Biopolymers* **2016**, *105* (1), 21–34.
- (42) Graham, S. E.; Leja, N.; Carlson, H. A. MixMD Probeview: Robust Binding Site Prediction from Cosolvent Simulations. *J. Chem. Inf. Model.* **2018**, *58* (7), 1426–1433.
- (43) Ghanakota, P.; DasGupta, D.; Carlson, H. A. Free Energies and Entropies of Binding Sites Identified by MixMD Cosolvent Simulations. *J. Chem. Inf. Model.* **2019**, *59* (5), 2035–2045.
- (44) DasGupta, D.; Chan, W. K. B.; Carlson, H. A. Computational Identification of Possible Allosteric Sites and Modulators of the SARS-CoV-2 Main Protease. *J. Chem. Inf. Model.* **2022**, *62* (3), 618–626.
- (45) DasGupta, D.; Mehrani, R.; Carlson, H. A.; Sharma, S. Identifying Potential Ligand Binding Sites on Glycogen Synthase Kinase 3 Using Atomistic Cosolvent Simulations. *ACS Appl. BioMater.* **2024**, *7* (2), 588–595.
- (46) Ghanakota, P.; van Vlijmen, H.; Sherman, W.; Beuming, T. Large-Scale Validation of Mixed-Solvent Simulations to Assess Hotspots at Protein–Protein Interaction Interfaces. *J. Chem. Inf. Model.* **2018**, *58* (4), 784–793.
- (47) Yuan, X.; Chinnaswamy, K.; Stuckey, J. A.; Yang, C.-Y. Computational Cosolvent Mapping Analysis Leads to Identify Salicylic Acid Analogs as Weak Inhibitors of ST2 and IL33 Binding. *J. Phys. Chem. B* **2022**, *126* (12), 2394–2406.
- (48) Thomas, C.; Bazan, J. F.; Garcia, K. C. Structure of the activating IL-1 receptor signaling complex. *Nat. Struct. Mol. Biol.* **2012**, *19* (4), 455–457.
- (49) Günther, S.; Sundberg, E. J. Molecular Determinants of Agonist and Antagonist Signaling through the IL-36 Receptor. *J. Immunol.* **2014**, *193* (2), 921–930.
- (50) Chemical Computing Group Inc. *Molecular Operating Environment(MOE) Version 2022.10*; Chemical Computing Group Inc: Montreal QC Canada 2022.
- (51) Case, D. A.; Aktulga, H. M.; Belfon, K.; Ben-Shalom, I. Y.; Berryman, J. T.; Brozell, S. R.; Cerutti, D. S.; Cheatham, T. E.; Cisneros, I. G. A.; Cruzeiro, V. W. D. et al. *Amber22*; University of California: San Francisco 2022.
- (52) Lexa, K. W.; Goh, G. B.; Carlson, H. A. Parameter Choice Matters: Validating Probe Parameters for Use in Mixed-Solvent Simulations. *J. Chem. Inf. Model.* **2014**, *54* (8), 2190–2199.
- (53) Maier, J. A.; Martinez, C.; Kasavajhala, K.; Wickstrom, L.; Hauser, K. E.; Simmerling, C. ff14SB: Improving the Accuracy of Protein Side Chain and Backbone Parameters from ff99SB. *J. Chem. Theory Comput.* **2015**, *11* (8), 3696–3713.
- (54) Ghanakota, P.; Carlson, H. A. Moving Beyond Active-Site Detection: MixMD Applied to Allosteric Systems. *J. Phys. Chem. B* **2016**, *120* (33), 8685–8695.
- (55) Martínez-Rosell, G.; Lovera, S.; Sands, Z. A.; De Fabritiis, G. PlayMolecule CrypticScout: Predicting Protein Cryptic Sites Using Mixed-Solvent Molecular Simulations. *J. Chem. Inf. Model.* **2020**, *60* (4), 2314–2324.
- (56) Salomon-Ferrer, R.; Götz, A. W.; Poole, D.; Le Grand, S.; Walker, R. C. Routine Microsecond Molecular Dynamics Simulations with AMBER on GPUs. 2. Explicit Solvent Particle Mesh Ewald. *J. Chem. Theory Comput.* **2013**, *9* (9), 3878–3888.
- (57) Ryckaert, J.-P.; Ciccotti, G.; Berendsen, H. J. C. Numerical integration of the cartesian equations of motion of a system with constraints: Molecular dynamics of n-alkanes. *J. Comput. Phys.* **1977**, *23* (3), 327–341.
- (58) Roe, D. R.; Cheatham, T. E., III PTRAJ and CPPTRAJ: Software for Processing and Analysis of Molecular Dynamics Trajectory Data. *J. Chem. Theory Comput.* **2013**, *9* (7), 3084–3095.
- (59) Lexa, K. W.; Carlson, H. A. Improving protocols for protein mapping through proper comparison to crystallography data. *J. Chem. Inf. Model.* **2013**, *53* (2), 391–402.
- (60) Schrödinger LLC. *The PyMOL Molecular Graphics System 2.0*; Schrödinger LLC. 2020.
- (61) Ester, M.; Kriegel, H.-P.; Sander, J.; Xu, X. A density-based algorithm for discovering clusters in large spatial databases with noise. In *The Second International Conference on Knowledge Discovery and Data Mining*, CiNii 1996; pp 226231.
- (62) Trott, O.; Olson, A. J. AutoDock Vina: Improving the speed and accuracy of docking with a new scoring function efficient optimization and multithreading. *J. Comput. Chem.* **2010**, *31* (2), 455–461.
- (63) Mai, T. T.; Phan, M.-H.; Thai, T. T.; Lam, T.-P.; Lai, N. V.-T.; Nguyen, T.-T.; Nguyen, T.-V.-P.; Vo, C.-V. T.; Thai, K.-M.; Tran, T.-D. Discovery of novel flavonoid derivatives as potential dual inhibitors against  $\alpha$ -glucosidase and  $\alpha$ -amylase: Virtual screening synthesis and biological evaluation. *Mol. Diversity* **2024**, *28* (3), 1629–1650.
- (64) Lam, T.-P.; Nguyen, D.-N.; Mai, T. T.; Tran, T.-D.; Le, M.-T.; Huynh, P. N. H.; Nguyen, D.-T.; Tran, V.-H.; Trinh, D.-T.-T.; Truong, P.; et al. Exploration of chalcones as 3-chymotrypsin-like protease (3CLpro) inhibitors of SARS-CoV-2 using computational approaches. *Struct. Chem.* **2022**, *33* (5), 1707–1725.
- (65) He, X.; Man, V. H.; Yang, W.; Lee, T.-S.; Wang, J. A fast and high-quality charge model for the next generation general AMBER force field. *J. Chem. Phys.* **2020**, *153* (11), 114502.
- (66) Wang, J.; Wang, W.; Kollman, P. A.; Case, D. A. Automatic atom type and bond type perception in molecular mechanical calculations. *J. Mol. Graphics Modell.* **2006**, *25* (2), 247–260.
- (67) Bouyssel, C.; Fiorucci, S. ProLIF: A library to encode molecular interactions as fingerprints. *J. Cheminf.* **2021**, *13* (1), 72.

- (68) Miller, B. R., III; McGee, T. D., Jr.; Swails, J. M.; Homeyer, N.; Gohlke, H.; Roitberg, A. E. MMPBSA.py: An Efficient Program for End-State Free Energy Calculations. *J. Chem. Theory Comput.* **2012**, *8* (9), 3314–3321.
- (69) González-Alemán, R.; Hernández-Castillo, D.; Caballero, J.; Montero-Cabrera, L. A. Quality Threshold Clustering of Molecular Dynamics: A Word of Caution. *J. Chem. Inf. Model.* **2020**, *60* (2), 467–472.
- (70) Diedrich, K.; Krause, B.; Berg, O.; Rarey, M. PoseEdit: Enhanced ligand binding mode communication by interactive 2D diagrams. *J. Comput.-Aided Mol. Des.* **2023**, *37* (10), 491–503.
- (71) Vigers, G. P.; Anderson, L. J.; Caffes, P.; Brandhuber, B. J. Crystal structure of the type-I interleukin-1 receptor complexed with interleukin-1 $\beta$ . *Nature* **1997**, *386* (6621), 190–194.
- (72) Dinarello, C. A.; Simon, A.; van der Meer, J. W. M. Treating inflammation by blocking interleukin-1 in a broad spectrum of diseases. *Nat. Rev. Drug Discovery* **2012**, *11* (8), 633–652.
- (73) Lal Gupta, P.; Carlson, H. A. Cosolvent Simulations with Fragment-Bound Proteins Identify Hot Spots to Direct Lead Growth. *J. Chem. Theory Comput.* **2022**, *18* (6), 3829–3844.
- (74) Brenke, R.; Kozakov, D.; Chuang, G.-Y.; Beglov, D.; Hall, D.; Landon, M. R.; Mattos, C.; Vajda, S. Fragment-based identification of druggable ‘hot spots’ of proteins using Fourier domain correlation techniques. *Bioinformatics* **2009**, *25* (5), 621–627.
- (75) Ngan, C.-H.; Hall, D. R.; Zerbe, B.; Grove, L. E.; Kozakov, D.; Vajda, S. FTSite: High accuracy detection of ligand binding sites on unbound protein structures. *Bioinformatics* **2012**, *28* (2), 286–287.
- (76) Bender, B. J.; Gahbauer, S.; Luttenb, A.; Lyu, J.; Webb, C. M.; Stein, R. M.; Fink, E. A.; Balius, T. E.; Carlsson, J.; Irwin, J. J.; et al. A practical guide to large-scale docking. *Nat. Protoc.* **2021**, *16* (10), 4799–4832.
- (77) Tran-Nguyen, V.-K.; Junaid, M.; Simeon, S.; Ballester, P. J. A practical guide to machine-learning scoring for structure-based virtual screening. *Nat. Protoc.* **2023**, *18* (11), 3460–3511.
- (78) Stein, R. M.; Yang, Y.; Balius, T. E.; O'Meara, M. J.; Lyu, J.; Young, J.; Tang, K.; Shoichet, B. K.; Irwin, J. J. Property-Unmatched Decoys in Docking Benchmarks. *J. Chem. Inf. Model.* **2021**, *61* (2), 699–714.
- (79) Imrie, F.; Bradley, A. R.; Deane, C. M. Generating property-matched decoy molecules using deep learning. *Bioinformatics* **2021**, *37* (15), 2134–2141.
- (80) Lingel, A.; Weiss, T. M.; Niebuhr, M.; Pan, B.; Appleton, B. A.; Wiesmann, C.; Bazan, J. F.; Fairbrother, W. J. Structure of IL-33 and Its Interaction with the ST2 and IL-1R $\alpha$ C $\beta$  Receptors—Insight into Heterotrimeric IL-1 Signaling Complexes. *Structure* **2009**, *17* (10), 1398–1410.
- (81) Smith, R. D.; Carlson, H. A. Identification of Cryptic Binding Sites Using MixMD with Standard and Accelerated Molecular Dynamics. *J. Chem. Inf. Model.* **2021**, *61* (3), 1287–1299.
- (82) Wanner, J.; Fry, D. C.; Peng, Z.; Roberts, J. Druggability assessment of protein-protein interfaces. *Future Med. Chem.* **2011**, *3* (16), 2021–2038.